Journal of
Marine Science and Engineering

MDPI

Article

Field Measurement and Theoretical Analysis of Sidewall Roughness on Shaft Resistance of Rock-Socketed Piles

Jun Liu [1,2], Zhongwei Li [1,2], Guoliang Dai [1,2,*] and Weiming Gong [1,2]

[1] Key of Laboratory for Concrete and Prestressed Concrete Structures of Ministry of Education, Southeast University, Nanjing 210096, China
[2] School of Civil Engineering, Southeast University, Nanjing 210096, China
* Correspondence: daigl@seu.edu.cn

Abstract: Sidewall roughness is a key factor influencing the shaft resistance of rock-socketed piles. Owing to the difficulties in onsite measuring and the inconsistency in quantitatively characterizing the roughness degree of sidewalls, existing approaches for estimating the shaft resistance of rock-socketed piles often cannot take this factor into account. Based on the measured surface curves of the 68 sockets in No. 6# and 7# group piles of the Chishi Bridge on the Ru-Chen Expressway in China, sidewall roughness is described by introducing the roughness factor (*RF*) based on the Horvath and Monash models, respectively, while a statistical analysis of the sidewall roughness in rock-socketed sections is also conducted. In addition, an analytical solution to the shaft resistance of rock-socketed piles with consideration of sidewall roughness and the relative settlement of the pile–rocks interface (Δs), is proposed and further compared with the field load tests. The results showed that: the *RF* obtained by the Horvath model is bigger than that obtained by the Monash model; the larger *RF* is, the bigger the mobilized shaft resistance; the analytical solution generally overestimates the mobilized shaft resistance of rock-socketed piles under the same Δs, and the deviation is less than 15% if Δs is larger than 3.00 mm. The Horvath model is recommended to quantitatively characterize the roughness degree of sidewalls for its good operability in practice.

Keywords: rock-socketed piles; sidewall roughness; shaft resistance; field load tests; Horvath and Monash models

Citation: Liu, J.; Li, Z.; Dai, G.; Gong, W. Field Measurement and Theoretical Analysis of Sidewall Roughness on Shaft Resistance of Rock-Socketed Piles. *J. Mar. Sci. Eng.* **2023**, *11*, 1622. https://doi.org/10.3390/jmse11081622

Academic Editor: Dong-Sheng Jeng

Received: 28 July 2023
Revised: 9 August 2023
Accepted: 14 August 2023
Published: 19 August 2023

1. Introduction

At the end of the 19th century, the Yugoslav scholar J. Cvijic used the name of the Karst Plateau (along the northern coast of the Adriatic Sea) to describe the landform and hydrological phenomena of limestone [1]. Carbonate rocks, such as limestone and dolomite, are widely distributed in coastal and offshore areas around the world. Compared with inland areas, the water-rich and flowing characteristics of marine environments may significantly increase the development of karst geology. A cast-in-place pile is a deep foundation that is constructed by placing concrete in an excavated hole (often, reinforcing steel can be installed); to increase the bearing capacity and reduce the settlement, drilled piles are commonly socketed into rocks, i.e., rock-socketed piles [2]. Usually, in order to improve the lateral stiffness and reliability of a pile foundation, two or more single piles are connected by a pile cap to form a group pile foundation. If the construction site encounters karst geology, they can be further subdivided into karst rock-socketed piles. Nowadays, rock-socketed piles are being increasingly used in foundation engineering to support heavily loaded buildings and structures, such as high-rise buildings, long-span bridges and wind turbines [3]. Due to the inevitable compressibility of reinforced concrete piles and the magnitude difference in the displacement required to reach the ultimate bearing state, the shaft and base resistances cannot mobilize simultaneously [4–7], shaft resistance generally dominates at the service loads of rock-socketed piles and therefore is always a topic of large research interests [8–10].

For a long time, researchers have studied the shear mechanism of the pile–rock interface theoretically, experimentally and numerically, and meanwhile numbers of empirical relations have also been proposed to further interpret the observed shaft resistances, especially based on the results in field load tests; however, existing empirical relations are still far from being able to explain the bearing mechanism. This is because these methods are usually site-specific, specifically manifesting in the rock properties (e.g., unconfined compressive strength of intact rocks, σ_c and rock mass deformation modulus, E_m), the rock socket geometries (e.g., rock socket length, L and rock socket diameter, B), and the construction technologies. In addition, effects of the aforementioned factors are essentially not independent, which makes the bearing behaviors of rock-socketed piles very complex. One of the physical factors which has a significant influence on shaft resistance is socket roughness, and the importance of socket roughness to shaft resistance has been well recognized by researchers [11–13], for the shear behavior (slip, dilation, and shear) of the pile–rock interface depends largely on roughness degree of rock socket, and the pressure-dependent incremental hardening can significantly enhance the shearing resistance of two contacting interfaces [14]. In fact, the roughness of the socket walls will depend on both geological factors, particularly discontinuities, and the construction method used to form the socket [15]. So far, although numbers of roughness models are available, a consistent index to characterize the sidewall roughness degree of the pile socket is still yet to be explored. In addition, although the bearing capacity test is a common practice for rock-socketed piles in engineering applications, few researchers have measured the roughness degree of sidewalls due to the difficulties in surface measurement of pile sockets. As the compilers of one national standard (highway engineering), the authors also hope to incorporate this index into the vertical bearing capacity design formula of rock-socketed piles.

Therefore, it is very important to study the influence of sidewall roughness on the shaft resistance of rock-socketed piles. Based on the quantitative description methods of sidewall roughness in literature, this study statistically analyzes the sidewall roughness of 68 rock-socketed piles at No. 6# and 7# pile groups of the Chishi Bridge on the Ru-Chen Expressway in China. In addition, the sidewall surface is idealized as uniformly distributed triangular asperities. The influence of sidewall roughness on the shaft resistance of rock-socketed piles, with a consideration of relative settlement of pile-rocks interface (Δs), is then explored theoretically and meanwhile compared with field load tests.

2. Roughness Models of Socket Sidewall

Due to the internal cohesion of intact rocks and the non-integrity of jointed rock masses, the pore-forming process of rock-socketed piles will produce a rough surface on the socket sidewall, as shown in Figure 1. Pells et al. [11] first recognized the influence of different roughness degrees of sidewalls on the bearing characteristics of shaft resistance of rock-socketed piles, and proposed a set of criteria for empirically classifying sidewall roughness, as shown in Table 1.

Table 1. Roughness Classification [11].

Roughness Class	Descriptions
*R*1	Straight, smooth-sided socket, grooves or indentations less than 1.00 mm depth
*R*2	Grooves of depth 1~4 mm, width greater than 2 mm, at spacing 50~20 mm
*R*3	Grooves of depth 4~10 mm, width greater than 5 mm, at spacing 50~200 mm
*R*4	Grooves or undulations of depth > 10 mm, width > 10 mm, at spacing 50~200 mm

Figure 1. The rough surface of sidewall.

In addition, quantitative indicators to describe the roughness degree of sidewalls have also been proposed by researchers. For example, based on the measurement of sidewall roughness, Horvath [16,17] developed a roughness factor (*RF*) to account for the effects of sidewall roughness on the peak shaft roughness (f_s) of rock-socketed piles. The predictive model for *RF* is:

$$RF = \frac{\Delta r}{R} \cdot \frac{L_t}{L} \quad (1)$$

where Δr is the average radial expansion (asperity) of rock-socketed sections; L_t is the total travel length along the sidewall profile which accounts for the irregular texture of socket sidewalls; R is the nominal radius of rock socket; and L is the nominal length of rock socket (see Figure 2).

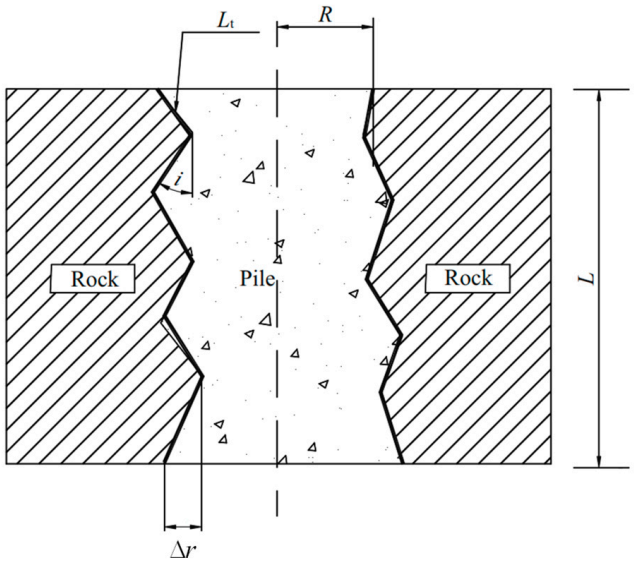

Figure 2. Identification of the sidewall roughness.

In fact, Equation (1) can be regarded as the product of two factors, i.e., $\Delta r/R$ and L_t/L, where $\Delta r/R$ is the relative depth of asperity of the socket surface, representing the radical changes of the sidewall; and L_t/L is the change of the socket wall along the depth direction, representing the overall shape of the sidewall. To calculate *RF*, the three parameters, L, L_t and R, can be directly obtained using a borehole logging system to measure the sidewall after the cleaning of the slurry suspension and soft soils accumulated at the bottom of the pile is finished, specifically, taking the actual socket depth of the rock-socketed section as L; and taking the average length of sidewall surface along the whole rock-socketed section as L_t; and taking the average radius of the sidewall along the whole rock-socketed section as R.

As to the last parameter, Δr, two models, namely, the Monash model [18] and the Horvath model [19], can be used to calculate the average radial expansion Δr of the rock-socketed section, as shown in Equations (2) and (3), and depicted in Figures 3 and 4, respectively.

$$\Delta r = \frac{1}{n}\sum_{i=1}^{n}|\Delta r_i| \tag{2}$$

$$\Delta r = \frac{1}{n}\sum_{i=1}^{n}\Delta r_i \tag{3}$$

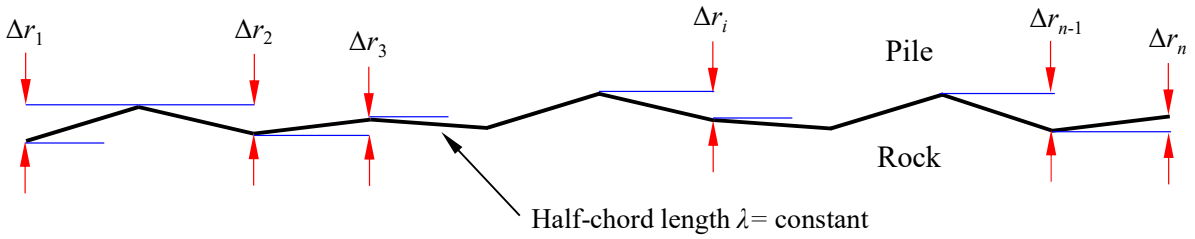

Figure 3. Monash roughness model (reproduced from Seidel and Collingwood [18]).

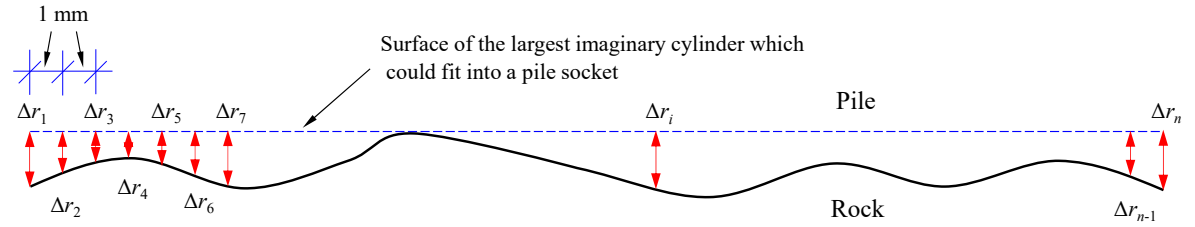

Figure 4. Horvath roughness model (reproduced from Horvath et al. [19]).

It should be noted that Δr, defined by the Horvath model, represents the average height of asperities which is measured with respect to the surface of the largest imaginary cylinder that can fit inside the rock socket. Although both the Monash model and the Horvath model have clear definitions, they are still inconvenient to use. An average and regular index to characterize the roughness degree of actual sidewalls is often needed, which is particularly true in a theoretical analysis. By comparing the empirical roughness classification proposed by Pells et al. [11] with the roughness factor proposed by Horvath [16,17], it can be seen that the mathematical significance of the latter one is clearer, because the *RF* can be calculated using Equation (1), and the four parameters involved here can be directly obtained by onsite measurement of pile sockets. Therefore, based on the measured sidewall curves of No. 6# and 7# pile groups in the Chishi Bridge on the Ru-Chen Expressway in China, the sidewall roughness (identified by *RF*) obtained by the Horvath and Monash models will be employed to statistically analyze the roughness degree in the rock-socketed sections.

3. Measured Results and Statistical Analysis of Socket Walls

3.1. Project Overview and Geological Conditions

The No. 6# and 7# cable towers in the Chishi Bridge on the Ru-Chen Expressway in China are supported by group pile foundations, which are bored cast-in-place rock-socketed piles by rotary drilling construction technologies. Since the bridge is located in karst areas, the geological condition of the bridge site is very complicated. The overall distribution and plane size of No. 6# and 7# group piles are the same, and the layout diagram of group pile foundation is shown in Figure 5.

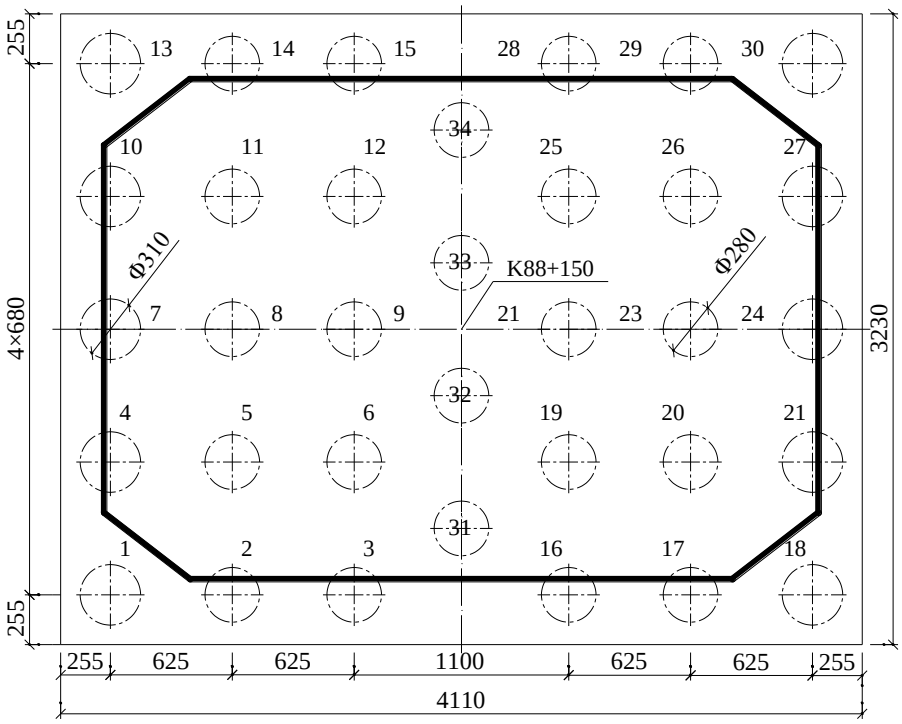

Figure 5. Layout of group pile foundation (units: cm).

According to the geological survey and drilling results, the flood plain and terrace of the bridge site are quaternary deposits, and the typical strata from new to old are:

1. Cover layers: including shallow planting soil, clay and boulder layer.
2. Limestone layer: karst is very developed and widely distributed in the bridge site, mainly in the form of ditches, troughs and caves, and the karst caves are recovered to exist at a larger depth. In general, the caves are often vertically developed, and the depth is about 60~70 m.
3. Structural rocks: the parent rock is limestone, and distributed in the F4 fault zone.

The recommended mechanical indexes of intact rocks and soil layers in the geological exploration report are shown in Table 2:

Table 2. Recommended mechanical indexes of soil and rock layers.

Geomaterials	$[\sigma_0]$/kPa	τ_i/kPa	f_{rk}/MPa
Clay	200~300	55~60	/
Erratic	400	100	/
Pebble	350	140	/
Weakly weathered marlstone	800	160	10
Strongly weathered carbonaceous limestone	800	150	6
Weakly weathered carbonaceous limestone	2000	300	10
Weakly weathered limestone	4000	600	40
Tectonic rocks (parent rock: limestone)	800	300	/

Note: $[\sigma_0]$ is the basic allowable value of foundation-bearing capacity; τ_i is the standard value of shaft resistance; f_{rk} is the uniaxial compressive strength of intact rocks.

3.2. Inspection Technology and Measured Results of Socket Walls

The GZ-2S digital borehole logging system (See Figure 6, the numbers in this figure represent the transmission or reception path of signals) is used to measure the borehole data of the No. 6# and 7# group piles including depth, verticality, diameter and sediments. Since the bearing capacity of rock-socketed piles is mainly provided by rock-socketed sections, only the results of rock-socketed sections are listed, as shown in Table 3.

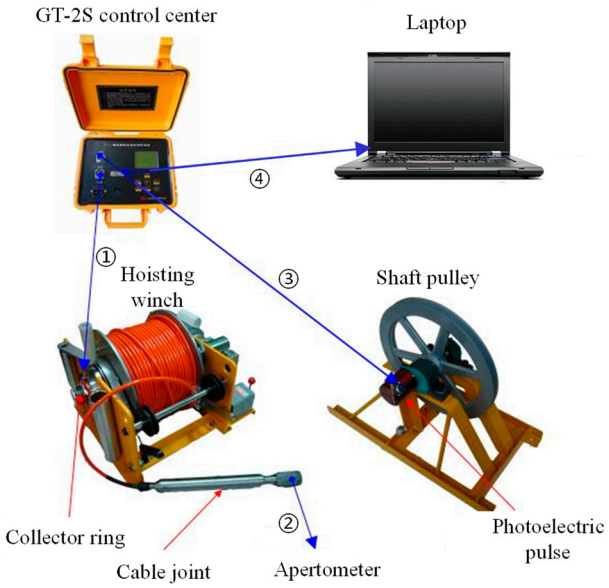

Figure 6. GZ-2S digital borehole logging system.

Table 3. Testing results of rock sockets in No. 6# and 7# group piles.

	6# Group Piles			7# Group Piles		
Socket No.	$\overline{R}$/mm	L_t/m	L/m	$\overline{R}$/mm	L_t/m	L/m
1	3200.84	126.21	102.45	2938.16	87.30	48.72
2	3040.61	107.45	67.67	3209.99	110.50	79.85
3	3209.54	139.48	74.87	3224.74	63.77	41.64
4	3217.54	50.71	37.29	3200.24	88.27	82.23
5	2959.73	65.92	47.87	3017.83	27.30	15.06
6	2994.56	80.21	52.06	3022.58	19.54	11.62
7	3214.44	60.38	38.99	3224.41	87.26	84.43
8	2986.30	96.63	63.36	2943.05	64.12	52.52
9	2989.72	33.17	19.63	2989.47	13.71	9.39
10	3188.72	26.39	25.71	3200.82	92.02	90.27
11	2962.72	73.23	50.03	3075.72	68.00	44.72
12	2971.75	69.49	50.00	3031.47	29.42	15.72
13	3155.65	13.88	11.25	3024.54	39.41	19.89
14	2948.23	64.38	44.82	3021.31	65.31	47.14
15	2999.63	35.91	14.36	3002.25	57.48	44.28
16	3063.08	169.67	58.86	3025.94	26.26	11.00
17	2991.61	77.41	39.19	3014.77	44.56	27.66
18	2949.72	30.34	18.86	2971.75	44.47	25.89
19	2987.27	70.92	30.50	3020.40	33.82	12.88
20	2982.72	46.75	34.52	3005.19	45.09	21.28
21	3056.90	62.24	30.32	2940.91	34.44	25.07
22	3075.16	44.58	26.55	3113.02	49.61	17.21
23	2980.67	61.58	40.02	2893.03	21.75	10.26
24	2975.40	55.86	39.75	3038.47	22.61	8.59
25	3040.87	70.96	33.03	3100.48	30.53	10.43
26	2981.94	16.36	9.92	3062.79	27.94	16.98
27	2964.58	42.24	33.21	2985.75	30.67	13.79
28	3087.32	52.52	30.32	3000.80	26.25	13.35
29	2948.23	56.17	32.08	3088.46	38.63	18.61
30	2893.35	33.03	21.86	2920.77	33.80	18.57
31	3222.49	45.89	30.63	3169.73	46.65	34.05
32	3236.71	59.55	59.52	3251.55	68.33	67.58
33	3190.71	34.78	31.51	3263.83	63.72	56.98
34	3204.54	85.82	60.62	3247.94	63.15	63.00

The graphics digitization software called Engauge Digitizer is employed to analyze the measured surface curves. According to the definition of Δr given by Seidel and Collingwood [18] and Horvath et al. [19], the *RF* of the rock-socketed sections is calculated, as shown in Table 4, and the comparison histograms of the *RF* obtained by the two models are shown in Figures 7 and 8, respectively.

Table 4. The *RF* of each sockets in No. 6# and 7# group piles.

No.	6# Group Piles				7# Group Piles			
	Horvath Model		Monash Model		Horvath Model		Monash Model	
	$\Delta\bar{r}$	*RF*	$\Delta\bar{r}$	*RF*	$\Delta\bar{r}$	*RF*	$\Delta\bar{r}$	*RF*
1	4.35	0.0017	5.72	0.0022	54.70	0.0334	26.37	0.0161
2	36.11	0.0189	30.91	0.0161	14.06	0.0061	10.81	0.0047
3	8.38	0.0049	11.87	0.0069	31.40	0.0149	20.00	0.0095
4	50.79	0.0215	21.22	0.0090	27.26	0.0091	10.56	0.0035
5	38.62	0.0180	27.00	0.0126	29.68	0.0178	34.77	0.0209
6	52.21	0.0269	38.61	0.0199	45.98	0.0256	18.44	0.0103
7	20.31	0.0098	14.69	0.0071	11.80	0.0038	6.90	0.0022
8	56.90	0.0291	31.30	0.0160	42.14	0.0175	25.09	0.0104
9	53.87	0.0304	27.87	0.0158	24.18	0.0118	27.57	0.0135
10	46.59	0.0150	18.96	0.0061	29.94	0.0095	11.22	0.0036
11	38.99	0.0193	22.78	0.0113	30.11	0.0149	35.58	0.0176
12	34.99	0.0164	31.64	0.0148	43.53	0.0269	47.32	0.0292
13	19.05	0.0074	13.55	0.0053	36.81	0.0241	17.38	0.0114
14	45.95	0.0224	25.25	0.0123	57.24	0.0262	23.10	0.0106
15	58.79	0.0490	38.69	0.0323	100.28	0.0434	34.23	0.0148
16	34.60	0.0326	31.18	0.0293	142.15	0.1121	95.90	0.0757
17	68.57	0.0453	47.18	0.0312	51.50	0.0275	36.97	0.0198
18	64.28	0.0351	26.05	0.0142	35.55	0.0205	35.66	0.0206
19	32.63	0.0254	27.83	0.0217	51.33	0.0446	74.67	0.0649
20	27.62	0.0125	11.44	0.0052	67.91	0.0479	54.80	0.0386
21	63.32	0.0425	62.93	0.0423	56.12	0.0262	39.61	0.0185
22	59.83	0.0327	45.47	0.0248	55.29	0.0512	69.78	0.0646
23	71.37	0.0368	38.40	0.0198	44.84	0.0329	48.81	0.0358
24	28.98	0.0137	25.70	0.0121	48.61	0.0421	40.24	0.0349
25	46.34	0.0327	35.10	0.0248	38.79	0.0366	40.11	0.0379
26	61.96	0.0343	27.90	0.0154	28.01	0.0150	21.48	0.0115
27	37.47	0.0161	31.78	0.0136	67.52	0.0503	34.25	0.0255
28	65.83	0.0369	40.71	0.0228	76.79	0.0503	61.31	0.0402
29	68.54	0.0407	46.18	0.0274	37.76	0.0254	56.65	0.0381
30	26.01	0.0136	47.91	0.0250	48.22	0.0300	20.24	0.0126
31	24.43	0.0114	30.42	0.0141	34.70	0.0150	16.71	0.0072
32	1.99	0.0006	3.19	0.0010	2.36	0.0007	4.90	0.0015
33	22.61	0.0078	17.57	0.0061	15.32	0.0052	12.92	0.0044
34	6.89	0.0030	9.18	0.0041	1.49	0.0005	4.20	0.0013

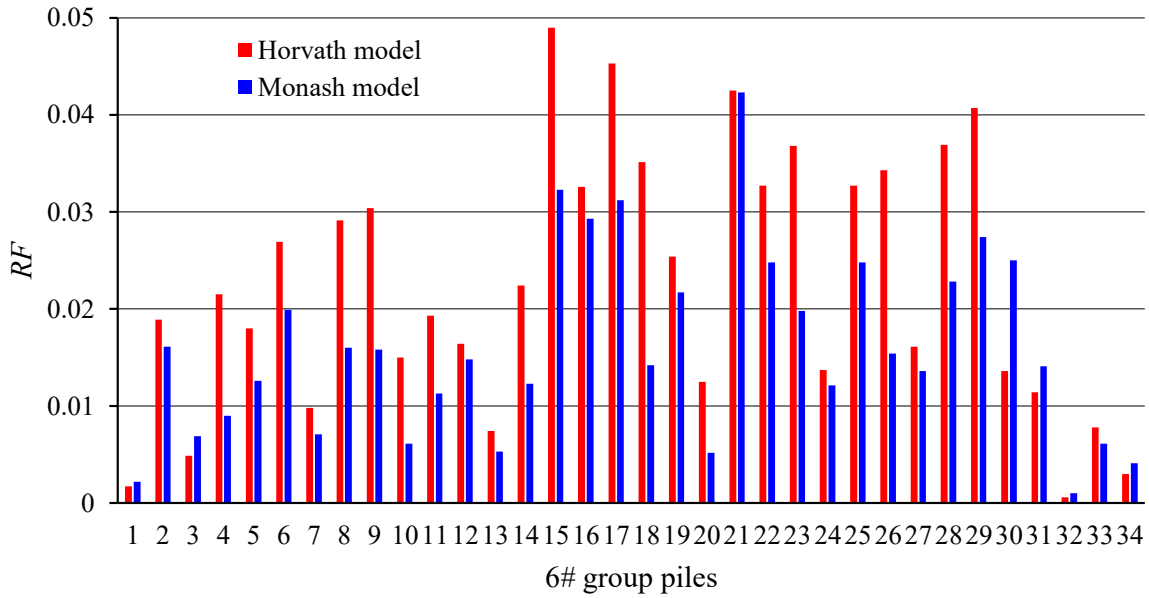

Figure 7. Contrast diagram of *RF* in No. 6# group piles.

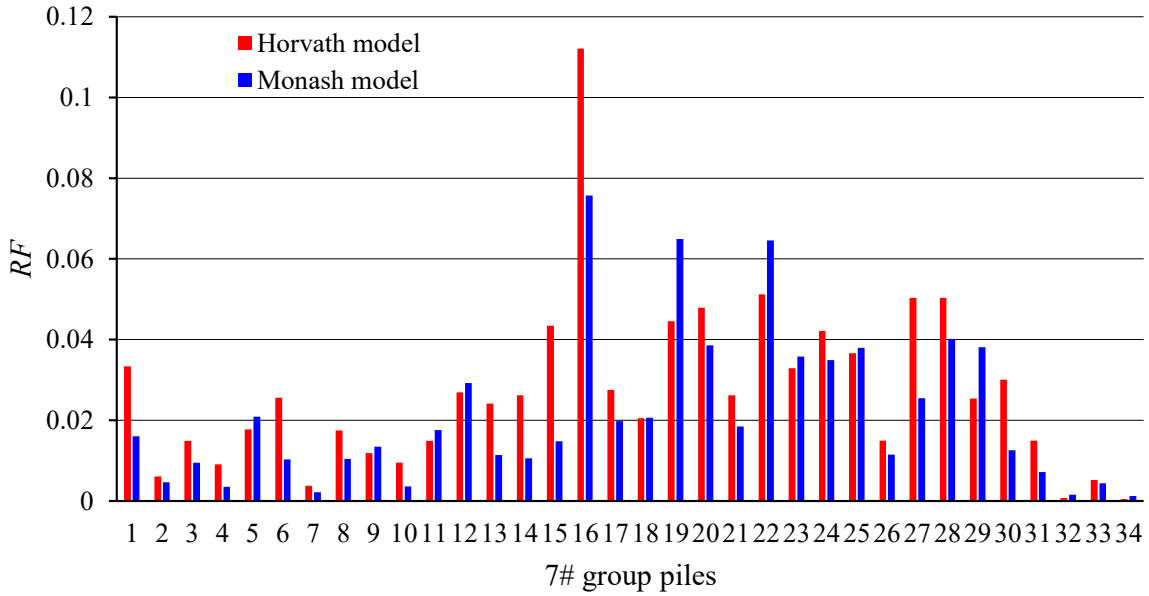

Figure 8. Contrast diagram of *RF* in No. 7# group piles.

The geometry of typical socket curves is shown in Figure 9 (wherein the left shows the 16th socket in No. 6# group piles with B = 2.8 m, L = 54.50 m; and the right shows the 20th socket in No. 7# group piles with B = 2.8 m, L = 48.50 m). It can be seen that the surface curve of the former in the covering layer is relatively uneven and the lower part is extremely rough, because the covering layer consists of pebbles and boulders, while the lower part belongs to the karst-developed area, and karst ditches exist for the whole length along the lower drilling holes. At the same time, the surface curve of the latter in the covering layer is relatively uniform, but the lower part is extremely rough, because the covering layer consists of planting soils and silty sands, while the lower part belongs to the karst-developed area, and a karst ditch or cave appears to exist at a level of about 42~46 m.

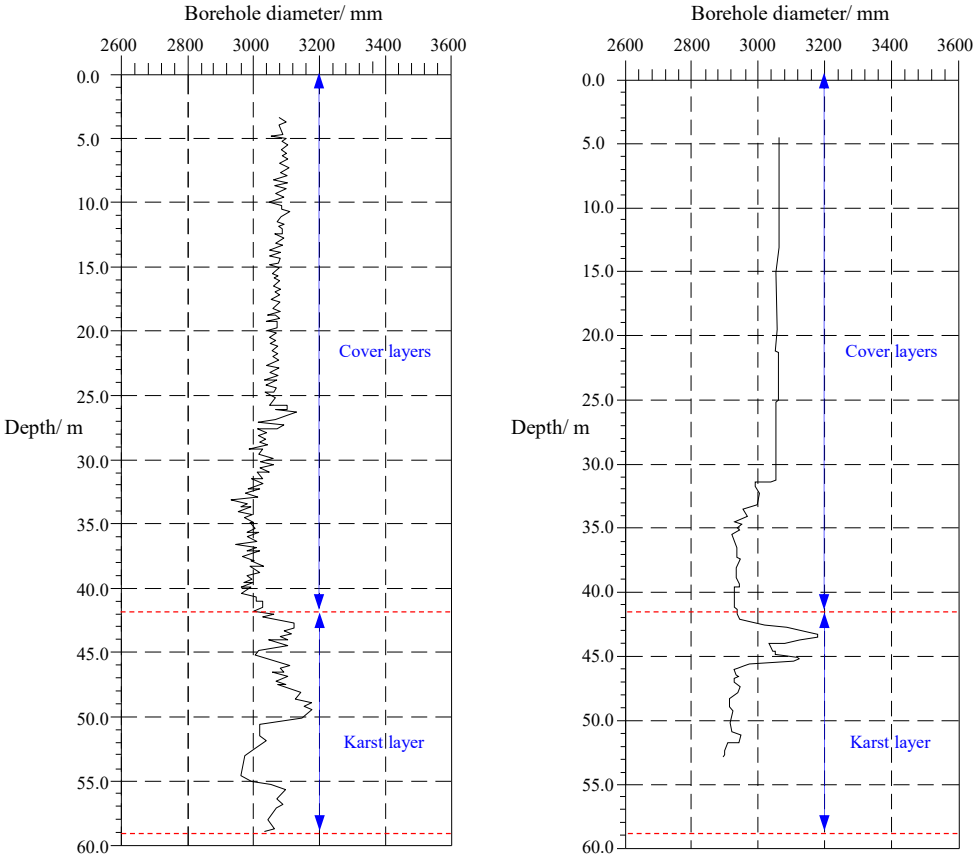

Figure 9. The typical surface curves of the 16th socket in No. 6# group piles (**left**) and the 20th socket in No. 7# group piles (**right**).

3.3. Statistical Analysis of Sidewall Roughness of Rock-Socketed Sections

According to the obtained *RF* in Section 3.2 (depicted in Figures 7 and 8, respectively), it can be concluded that the average *RF* obtained by the Monash model is much smaller than that obtained by the Horvath model. This is because the Horvath model is calculated from the largest imaginary cylinder that can fit inside the rock socket when calculating the average radial expansion Δr, while the Monash model idealizes the sidewall surface as a set of turning curves and calculates the average distance of each line. The comparison between the two models is shown in Table 5.

Table 5. Comparison between the Horvath model and Monash model in rock-socketed sections.

	6#			7#		
	Average	**Max**	**Min**	**Average**	**Max**	**Min**
Horvath model	0.0225	0.0490	0.0006	0.0270	0.1121	0.0005
Monash model	0.0160	0.0423	0.0010	0.0215	0.0757	0.0013

Although the *RF* values calculated by the Monash and Horvath models are different, which could be specifically recognized from Figure 7, the maximum values in the No. 6# group piles are the 15th and 21st holes, and the minimum value is the 32nd hole. The *RF* value of each socket of the No. 6# group piles obtained by the two models is roughly similar. For No. 7# group piles depicted in Figure 8, the minimum *RF* obtained under the two models is the 34th hole, and the maximum *RF* is the 16th hole. The *RF* in the rock-socketed sections of the No. 6# and 7# group piles under different roughness intervals is counted, as shown in Table 6:

Table 6. Roughness intervals of the No. 6# and 7# group piles.

	Monash Model	Horvath Model
$0 < RF \leq 0.02$	45	31
$0.02 < RF \leq 0.04$	18	25
$RF > 0.04$	5	12

The Δr defined in the Monash and Horvath model is different in each case, and Δr is a key parameter used to calculate the RF of sidewalls of rock-socketed piles. For a rock sidewall with a uniform surface, the difference of the two models may result in a slight variation of RF values, but if the sidewall surface changes unevenly and greatly at different depths, e.g., karst layers, the Horvath model results will be larger. Table 6 also verifies that the RF value obtained by the Horvath model is higher than that obtained by the Monash model. The socket curves can be generally divided into three categories:

(1) $0 < RF \leq 0.02$: this kind of socket roughness belongs to $R1$, indicating that the sidewall is straight and smooth, karst layers can hardly be encountered within this roughness interval, and the RF is much lower than the average level.
(2) $0.02 < RF \leq 0.04$: this kind of socket roughness changes in different strata, and specifically, in the karst layer, the sidewall surface is significantly rough, and the socket roughness belongs to $R3$ or $R4$. However, after passing through the karst layer, the sidewall surface is relatively uniform and the roughness belongs to $R3$.
(3) $RF > 0.04$: this kind of socket roughness belongs to $R4$, and the grooves or undulations of depth is much larger than 10 mm, indicating that the karst layer is strongly developed.

4. Shaft Resistance of Rock-Socketed Piles Considering Sidewall Roughness

4.1. Empirical Models

For a long time, empirical methods for predicting the shaft resistance of rock-socketed piles have typically related to the unconfined compressive strength of intact rocks (σ_c) through the results of pile load tests, and the shaft resistance in these empirical formulas often refers only to the peak shaft resistance. The common limitations of this approach can be summarized into two aspects: (1) the sidewall roughness often cannot be considered; (2) the relative displacement at the pile–rock interface cannot be involved. To quantify the effect of sidewall roughness on the shaft resistance of rock-socketed piles, the roughness classification proposed by Pells et al. [11] are incorporated into the design method by Rowe and Armitage [15] as below:

$$f_s = (0.45 \sim 0.60)\sqrt{\sigma_c} \quad (4)$$

where f_s is the pile shaft resistance, kPa; σ_c is the uniaxial compressive strength of intact rocks, kPa. According to Rowe and Armitage [15], in Equation (4), for clean regular sockets (roughness $R1$, $R2$ and $R3$), 0.45 can be used; and for clean rough sockets (roughness $R4$), then 0.60 can be used.

Additionally, to quantify the influence of roughness, Horvath et al. [19] proposed an empirical correlation between the pile shaft resistance and the RF based on model tests as follows:

$$f_s = 0.8\sigma_c(RF)^{0.45} \quad (5)$$

4.2. Theoretical Model

The empirical models mentioned above indeed consider the influence of sidewall roughness, but they cannot predict the instantaneous shaft resistance, i.e., the mobilized shaft resistance under different relative displacement at the pile–rock interface (Δs). Due to the high bearing capacity of rock-socketed piles, at the service loads, the shaft resistance along the whole length of pile can hardly reach the ultimate state at the same time, thus, an analytical solution to the shaft resistance with consideration of RF and Δs, can give a better understanding of the load transfer mechanism along the depth of rock-socketed piles.

The beneficial effect of socket roughness is a combined consequence of the dilational nature of a rough concrete–rock interface and the constant normal stiffness (CNS) boundary condition which governs the normal stress at the concrete–rock interface. The pile–rock interface is usually simplified into a plane stress problem with a set of regular triangular asperities in theoretical studies [20–23]. The present study follows the same idea, and specifically, the socket sidewall profile is simplified as triangular asperities, and micro-mechanical analysis is performed on the shear behavior of one representative asperity, which is depicted in Figure 10, and the triangle asperity can be quantitatively characterized by three geometric parameters, i.e., roughness angle β, half-chord length λ and chord height h, and the relationship between the three parameters is:

$$h = \lambda \tan \beta \tag{6}$$

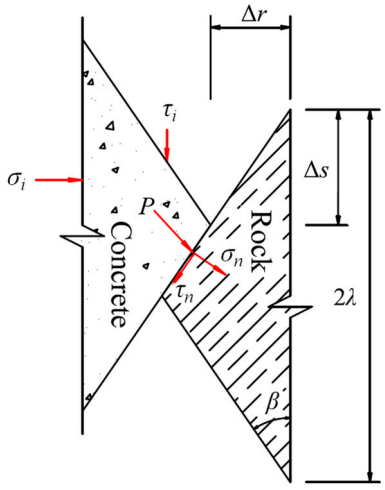

Figure 10. Stress state of a triangular asperity on pile-rocks interface.

Since h, λ and β can change along the depth of a pile, the average values of those three individual parameters within a specific distance can be used. The average expansion of the sidewall radius Δr obtained by the Horvath model is:

$$\Delta r = 0.5\lambda \tan \beta \tag{7}$$

Substituting Equation (7) into (1) yields

$$RF = \frac{0.5\lambda \tan \alpha}{R \cos \alpha} \tag{8}$$

The relative displacement Δs of the pile–rock interface and the radial deformation ΔR of the rock-socketed piles due to dilatancy effect should satisfy the geometric relationship.

$$\Delta s = \Delta R \cot \beta \tag{9}$$

The average separation of the pile–rock interface (Δh) caused by the dilatancy effect is:

$$\Delta h = \frac{\Delta s}{\sqrt{1 + \cot^2 \beta}} = \frac{\Delta R \cot \beta}{\sqrt{1 + \cot^2 \beta}} \tag{10}$$

The shaft resistance of rock-socketed piles can be easily determined by establishing the force equilibrium equations of the triangular asperity depicted in Figure 10. Compared with the rock masses of different weathering degrees around a pile socket, the reinforced concrete pile is ideally regarded as a rigid material, and under this circumstance, the failure of the pile-rock interface will only take place inside rock masses. Additionally, the normal

stiffness K of the sidewall is assumed to remain unchanged (CNS) during the shear process of the pile–rock interface. The equilibrium equation along the direction of separation displacement Δh (i.e., normal stress σ_{n}) can be expressed as:

$$\sigma_i \cdot 2\lambda \cos\beta + \tau_i \cdot 2\lambda \sin\beta = K\Delta h \cdot \frac{\lambda}{\cos\beta} \tag{11}$$

where K is the global normal stiffness of surrounding rock masses and is assumed to be constant, and it can be obtained through the reaming theory of an infinite cylindrical hole:

$$K = \frac{E}{(1+\mu)B} \tag{12}$$

where B is pile diameter, m; μ is Poisson's ratio; E is elastic modulus, GPa, and E can be estimated following Hoek and Diederichs [24]:

$$E = 100\left[\frac{1-D}{1+\mathrm{e}^{(75+25D-GSI)/11}}\right] \tag{13}$$

where GSI is the Geological Strength Index defined by Hoek and Karakas [25], and D is the disturbance factor included in the Hoek–Brown criterion [26].

As the shear deformation Δs of the pile–rock interface increases, the effective contact areas gradually decrease, resulting in an increase in the normal stress σ_{n} along the effective contact surfaces of the pile-rocks interface. Combining Equations (10) and (11), the normal stress σ_{n} can be obtained:

$$\sigma_{\mathrm{n}} = K\Delta h \cdot \frac{\lambda}{\lambda - \Delta s} = \frac{K\Delta s}{\sqrt{1+\cot^2\beta}} \cdot \frac{\lambda}{\lambda - \Delta s} \tag{14}$$

Along the direction of tangential stress τ_{n}, the equilibrium equation can be expressed as:

$$\tau_i \cdot 2\lambda \cos\beta - \sigma_i \cdot 2\lambda \sin\beta = \tau_{\mathrm{n}} \cdot \frac{\lambda - \Delta s}{\cos\beta} \tag{15}$$

The relationship between normal stress σ_{n} and tangential stress τ_{n} of the triangular asperity is:

$$\sigma_{\mathrm{n}} = \tau_{\mathrm{n}} \tan\left(\beta + \arctan\frac{\sigma_i}{\tau_i}\right) \tag{16}$$

For a given shear deformation Δs, the average shear stress τ_i and the average compressive stress σ_i at the pile–rock interface can be easily obtained by solving Equations (11), (15) and (16). So far, the influence of the effects of pile–rock surface roughness, with a consideration of relative settlement of pile–rock interface (Δs) on the shaft resistance of rock-socketed piles has been clarified.

5. Validation and Analysis

The vertical static load test was conducted on a fully-instrumented engineering pile, i.e., the 12th pile in the No. 6# group piles (see Table 7), by the self-balanced method (also called O-cell load testing method). The measuring apparatus and equipment, including steel bar meters, suspension devices and load cells, are preinstalled on the steel-reinforced cage of the testing pile at specific depths, thus, the pile axial force, shaft resistance and displacement of the testing pile at different depths during the loading process can be easily measured.

Table 7. Design parameters of the testing pile.

Concrete Grade	*B*/m	*L*/m	Planned Load/kN
C30	2.8	67.5	200,000

According to the geological survey, the bearing strata of the testing pile can be divided into three layers: the uppermost elevation of 265~245 m is the boulder layer; the middle elevation of 245~200 m is the interlaced karst layer of ditches and fissures; and the lower part (5 m deep until the pile tip) is the limestone layer. The rock mass at this depth has a high integrity and thus is selected as the bearing stratum of the pile tip. The load-shaft resistance response of the testing pile in the field load tests is shown in Figure 11, where the shaft resistance of the three layers is averaged, and the mobilized shaft resistance in the lower part is larger than that in the middle part, especially under the action of the last few levels of loads. Compared with the recommended mechanical indexes of soil and rock layers listed in Table 2, the observed shaft resistance of the testing pile is about two times the design expectation, indicating that the design of group piles foundation is very conservative.

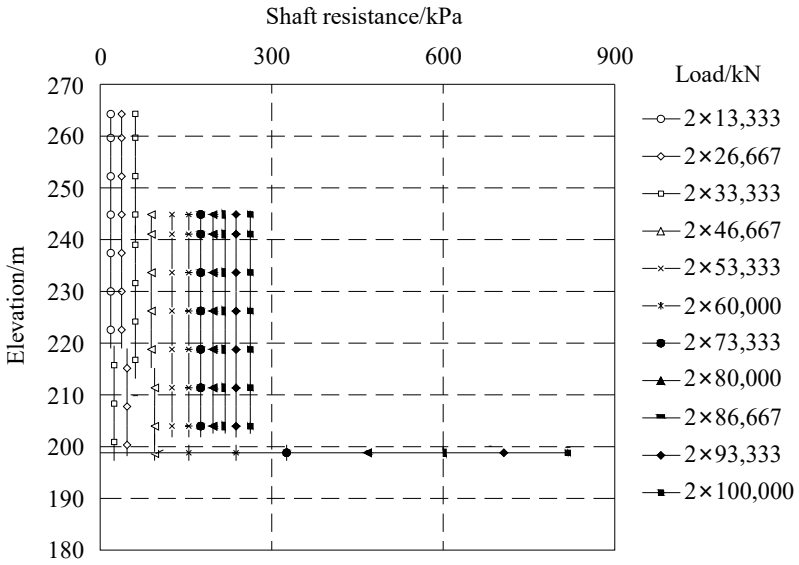

Figure 11. Load-shaft resistance response of the testing pile.

The measured sidewall *RF* of the second layer in the bearing strata is 0.0127, and since the second layer locates at the karst-developed areas, numbers of discontinuities exist near the bottom of this layer. According to the experience of practical engineering, that is, for the sake of engineering safety, determination of the bearing capacity of rock-socketed piles in existing geological conditions will largely depend on field load tests, and the shaft resistance should artificially be reduced and even ignored in the actual design. The third layer belongs to conventional geological conditions, and therefore can be analyzed both experimentally and theoretically. It should be noted that, considering the influence of drilling speed, filling coefficient and borehole stability, the surface of socket wall in the third layer is artificially roughened, the measured sidewall *RF* of this layer is 0.0199, the half-chord length of asperities on the sidewall approximately equals 100 mm, and thus belongs to the *R*3 class. According to the drilling cores during the geological survey and the guidance of disturbance for different socket construction methods in AASHTO (2014) [27], *GSI* is determined as 45 and *D* is 0 in Equation (13) to estimate the elastic modulus of rock masses in the third layer.

Substituting the compressive strength of limestone and the measured sidewall *R*3 or *RF* into Equations (4) and (5), the peak shaft resistance based on the empirical correlation

proposed by Rowe and Armitage [15] is 1423 kPa, by Horvath et al. [19] is 1373 kPa, but the mobilized shaft resistance under the action of the last load level (equals to 2 × 10,000 kN) is only 800 kPa. Since the tested pile is selected from the engineering piles, the loading scheme should ensure that the tested pile cannot be loaded to the failure state, and from the developing trend of the tested shaft resistance verse relative displacement (Δs) depicted with blue line in Figure 12, the ultimate shaft resistance has yet to be mobilized at the end of the field test.

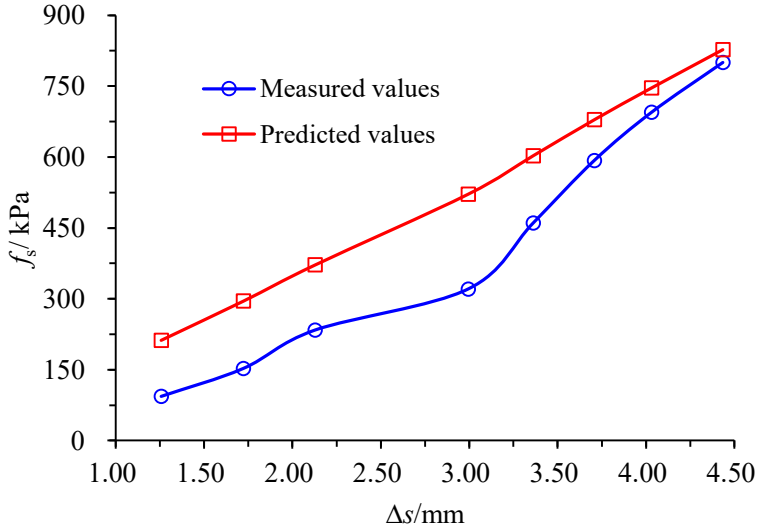

Figure 12. Measured and predicted shaft resistance f_s verse relative displacement Δs.

Based on the theoretical model discussed in Section 4.2, the estimated shaft resistance with a consideration of the sidewall roughness at different relative settlement of the pile–rock interface can be easily obtained, and also depicted with red line in Figure 12. It can be seen that, the theoretical model generally overestimates the shaft resistance compared to the field load test at the same Δs, and after the Δs reaches larger than 3.00 mm, the deviation is less than 15%. This may be caused by the "filter cake" on the pile–rock interface deposits from the wall-protecting slurry during the forming process of rock sockets, which is similar to a weak interlayer in layered rock masses. The filter cake can reduce the elastic modulus E used in Equation (12) to a certain extent, especially at the early stages of the field loading tests, at this time, the filter cake has not been fully compacted, and as a consequence, the surrounding rock masses can only provide a lower global stiffness to piles.

6. Conclusions

The design of piles socketed into rocks heavily depends upon the resistance along the shaft, particularly in the serviceability state. Sidewall roughness is identified as a key factor influencing the shaft resistance of rock-socketed piles. In this study, the sidewall roughness of 68 sockets in the No. 6# and 7# group piles foundation of the Chishi Bridge on the Ru-Chen Expressway in China were quantitively described by introducing the roughness factor (RF) respectively based on the Horvath model and the Monash model, and a statistical analysis of the sidewall roughness in the rock-socketed sections was also conducted. In addition, a micro-mechanical analysis was performed on the shear behavior of one representative asperity selected from the idealized triangular asperities at the pile–rock interface, and an analytical solution to the shaft resistance of rock-socketed piles with consideration of sidewall roughness and relative settlement of the pile–rock interface (Δs) was proposed and further compared with the field load tests. The following results from this study are drawn:

(1) Geological conditions have a significant effect on roughness degree of sidewalls, the *RF* in the rock-socketed section obtained by the Horvath model is bigger than that obtained by the Monash model, especially when piles pass through the karst layers.
(2) Field load tests show that the larger *RF* is, the bigger mobilized shaft resistance, but for karst layers, a reduction of shaft resistance needs to be considered for the sake of engineering safety.
(3) Compared with the mobilized shaft resistance in the field load tests, the analytical solution considering the roughness degree and relative settlement of the pile–rock interface generally overestimates the mobilized shaft resistance under the same Δs, and the deviation is less than 15% if Δs is larger than 3.00 mm.
(4) It is hoped that in future processes for field load tests of rock-socketed piles, the surface curves of rock sockets may be measured prior to load tests. With the development of field-testing data and theoretical studies, the roughness index can be incorporated into the vertical bearing capacity design formula of rock-socketed piles.

Author Contributions: Writing—original draft preparation, data curation, J.L.; conceptualization, writing—review and editing, Z.L. and G.D.; supervision, G.D. and W.G. All authors have read and agreed to the published version of the manuscript.

Funding: This work was supported by the National Natural Science Foundation of China (grant numbers 52208333, 51878160, 52078128), and the Jiangsu Province Excellent Postdoctoral Funding Program (grant number 2022ZB135).

Institutional Review Board Statement: Not applicable.

Informed Consent Statement: Not applicable.

Data Availability Statement: The authors confirm that all the data generated or analyzed during this study are included in this published article.

Conflicts of Interest: The authors declare no conflict of interest.

References

1. Liu, N.W. *Physical Geography*, 3rd ed.; Science Press: Beijing, China, 2014.
2. Zhang, L. *Drilled Shafts in Rock: Analysis and Design*; Balkema: London, UK, 2004.
3. Sagong, M.; Paik, K.; Kim, D. A new approach to estimate side resistance of rock socketed drilled shafts. *Soils Found.* **2007**, *47*, 415–421. [CrossRef]
4. Haberfield, C.; Collingwood, B. Rock-socketed pile design and construction: A better way? *Proc. Inst. Civ. Eng.-Geotech. Eng.* **2006**, *159*, 207–217. [CrossRef]
5. Woodward, R.J.; Gardner, W.S.; Greer, D.M. *Drilled Pier Foundations*; McGraw-Hill Book Co.: New York, NY, USA, 1972.
6. Mandolini, A.; Ramondini, M.; Russo, G.; Viggiani, C. Full scale loading tests on instrumented CFA piles. In *Deep Foundations 2002: An international Perspective on Theory, Design, Construction, and Performance*; American Society of Civil Engineers: Orlando, FL, USA, 2002; pp. 1088–1097.
7. O'Neil, M.W.; Reese, L.C. *Drilled Shafts: Construction Procedures and Design Methods*; Pub. No. FHWA-IF-99-025; Federal Highway Administration: Washington, DC, USA, 1999.
8. Murali, A.K.; Tran, K.M.; Haque, A.; Bui, H.H. Experimental and Numerical Investigation of the Load-Bearing Mechanisms of Piles Socketed in Soft Rocks. *Rock Mech. Rock Eng.* **2022**, *55*, 5555–5576. [CrossRef]
9. Asem, P.; Gardoni, P. On the Use and Interpretation of In Situ Load Tests in Weak Rock Masses. *Rock Mech. Rock Eng.* **2021**, *54*, 3663–3700. [CrossRef]
10. Dai, G.L.; Salgado, R.; ASCE, F.; Gong, W.M.; Zhu, M.X. The effect of sidewall roughness on the shaft resistance of rock-socketed piles. *Acta Geotech.* **2017**, *12*, 429–440. [CrossRef]
11. Pells, P.; Rowe, R.; Turner, R. An experimental investigation into side shear for socketed piles in sandstone. In Proceedings of the International Conference on Structural Foundations on Rock, Sydney, Australia, 7–9 May 1980; pp. 291–302.
12. Horvath, R.G. *Research Project Report on Load Transfer System for Rock-Socketed Drilled Pier Foundations. For the National Research Council of Canada, DSS File no. 10X5.31155-9-4420, Contract Serial No. lSX79.00531*; National Research Council of Canada: Ottawa, ON, Canada, 1980.
13. Rowe, R.K.; Armitage, H.H. *The Design of Piles Socketed into Weak Rock*; Research Report GEOT-11-84; Faculty of Engineering Science, The University of Western Ontario: London, ON, Canada, 1984.
14. Ashutosh, T. Estimating In Situ Deformation of Rock Masses Using a Hardening Parameter and RQD. *Int. J. Geomech.* **2012**, *13*, 348–364. [CrossRef]

15. Rowe, R.K.; Armitage, H.H. A design method for drilled piers in soft rock. *Can. Geotech. J.* **1987**, *24*, 126–142. [CrossRef]
16. Horvath, R.G. *Field Load Test Data on Concrete-to-Rock "Bond" Strength for Drilled Pier Foundations*; Department of Civil Engineering, University of Toronto: Toronto, ON, Canada, 1978; ISSN 0316-7968.
17. Horvath, R.G. Drilled Piers Socketed into Weak Shale-Methods of Improving Performance. Ph.D. Thesis, Department of Civil Engineering, University of Toronto, Toronto, ON, Canada, 1982.
18. Seidel, J.; Collingwood, B. A new socket roughness factor for prediction of rock socket shaft resistance. *Can. Geotech. J.* **2001**, *38*, 138–153. [CrossRef]
19. Horvath, R.; Kenney, T.; Kozicki, P. Methods of improving the performance of drilled piers in weak rock. *Can. Geotech. J.* **1983**, *20*, 758–772. [CrossRef]
20. Johnston, I.W.; Lam, T.S. Shear behavior of regular triangular concrete/rock joints—Analys is. *J. Geotech. Eng.* **1989**, *115*, 711–727. [CrossRef]
21. Hou, J.C.; Zhao, H.; Peng, W.Z.; Zhao, M.H. A limit solution for predicting side resistance on rock-socketed piles. *J. Eng. Mech.* **2022**, *148*, 04021131. [CrossRef]
22. Zhang, Q.Q.; Li, H.T.; Cui, W.; Zhao, Y.H.; Wang, S.L.; Xu, F. Analysis of grout diffusion of post grouting pile considering the time-dependent behavior of grout viscosity. *Int. J. Geomech.* **2021**, *21*, 04021201. [CrossRef]
23. Seidel, J.P.; Haberfield, C.M. A theoretical model for rock joints subjected to constant normal stiffness direct shear. *Int. J. Rock Mech. Min. Sci.* **2002**, *39*, 539–553. [CrossRef]
24. Hoek, E.; Diederichs, M.S. Empirical estimation of rock mass modulus. *Int. J. Rock Mech. Min. Sci.* **2006**, *43*, 203–215. [CrossRef]
25. Hoek, E.; Karakas, A. Practical rock engineering. *Environ. Eng. Geosci.* **2008**, *14*, 55–57.
26. Hoek, E.; Brown, E.T. Practical estimates of rock mass strength. *Int. J. Rock Mech. Min. Sci.* **1997**, *34*, 1165–1186. [CrossRef]
27. ASSHTO. *LRFD Bridge Design Specifications*, 7th ed.; American Association of Stata Highway and Transportation Officials: Washington, DC, USA, 2014.